

2. Landforms made by running water

2.1 Geomorphic action of running water

Major erosive action of running water is tractive force acting on bed surface.

Tractive force τ is given by

$$\tau = \rho ghS \quad (2.2)$$

where ρ is density of water, g is gravity acceleration, h is water depth and S is slope gradient. Tractive force is also represented by the relation

$$u_* = \sqrt{\tau / \rho} = \sqrt{ghS} \quad (2.3)$$

where u_* is friction velocity.

Many empirical relations which give the amount of sediment load transported by tractive action are presented so far. A simplified general form of the formulas is represented by

$$\frac{q_b}{u_* d} = f \left\{ \frac{u_*^2}{(\sigma / \rho - 1)gd} \right\} \quad (2.4)$$

where the left-hand side is tractional load in no-dimension and the term in the parenthesis of the right-hand side is tractive force in no-dimension. A representative one of this type is Brown's Equation:

$$\frac{q_b}{u_* d} = 10 \left(\frac{u_*^2}{(\sigma / \rho - 1)gd} \right)^2 \quad (2.5)$$

where q_b is tractional load per unit time and unit width, d is particle diameter, σ is density of the particle and ρ is density of the fluid.

By simplification, the following relation

$$q_b = c \tau^\alpha = c(\rho ghS)^\alpha \quad (2.6)$$

is derived, where c is proportional constant.

Continuity equation for tractional load is given by

$$\frac{\partial z}{\partial t} = - \frac{1}{1 - \lambda} \frac{\partial q_b}{\partial x} \quad (2.7)$$

where z is altitude, t is time, λ is porosity of sediment layer and x is horizontal distance.

Now, we consider the surface flow on mountain slopes caused by rainfall as shown in Fig.2.2. Equation of motion and equation of continuity in one dimension for the surface flow are

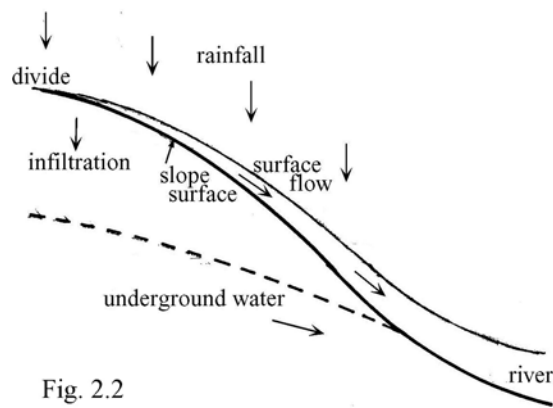


Fig. 2.2

$$\frac{1}{g} \frac{\partial v}{\partial t} + \frac{v}{g} \frac{\partial v}{\partial x} + \frac{\partial h}{\partial x} - S + \frac{n^2 v^2}{h^{4/3}} = 0 \quad (2.8)$$

$$\frac{\partial h}{\partial t} + \frac{\partial(vh)}{\partial x} = r \quad (2.9)$$

where v is flow velocity, h is flow depth, x is horizontal distance from divide, S is gradient of ground surface, r is lateral inflow by rainfall, n is Manning's coefficient of roughness. When we consider long-term geomorphic process, (2.8) and (2.9) can be simplified as

$$-S + \frac{n^2 v^2}{h^{4/3}} = 0 \quad (2.10)$$

$$\frac{d(vh)}{dx} = r \quad (2.11)$$

Combining the above fundamental equations, a partial differential equation which describes the evolution of longitudinal slope profile can be derived.

Solving the differential equation derived from (2.10) and (2.11) under the boundary condition $x=0$, $h=0$, and under the simplification that S is constant, flow depth h at the distance x from divide is given by

$$h = \left(\frac{nrx}{S^{1/2}} \right)^{3/5} \quad (2.12)$$

A generalized form of (2.5) is written as

$$\frac{q_b}{u_* d} = k \left(\frac{u_*^2}{(\sigma / \rho - 1)gd} \right)^m \quad (2.13)$$

Tractional load at x is obtained from (2.3), (2.12) and (2.13). Substituting the tractional load q_b into equation of continuity of sediment (2.7), the following partial differential equation which describes the evolution of longitudinal slope profile is

derived:

$$\frac{\partial z}{\partial t} = Ar^{0.6m+0.3} \left(0.35x^{0.6m+0.3} S^{0.7m-0.65} \frac{\partial S}{\partial x} + 0.3x^{0.6m-0.7} S^{0.7m+0.35} \right) \quad (2.14)$$

$$A = \frac{(2m+1)kdg^{m+0.5}n^{0.6m+0.3}}{(1-\lambda)\{(\sigma/\rho-1)gd\}^m}$$

The main variables are slope gradient, slope curvature and the distance from divide. Equation (2.14) can be rewritten as

$$\frac{\partial z}{\partial t} = K_1x^{0.6m+0.3} \left(\frac{\partial z}{\partial x} \right)^{0.7m-0.65} \frac{\partial^2 z}{\partial x^2} + K_2x^{0.6m-0.7} \left(\frac{\partial z}{\partial x} \right)^{0.7m+0.35} \quad (2.15)$$

In a steady state continuity equation (2.7) is

$$\frac{dq_b}{dx} = 0 \quad (2.16)$$

From (2.6), (2.12) and (2.16),

$$S = \frac{dz}{dx} = S_0x^{-6/7} \quad (2.17)$$

is derived, where z is altitude, x is horizontal distance from divide and S_0 is slope gradient at $x=0$. The relation shows that longitudinal valley profile is described by a power function of x in a steady state

2.2 Longitudinal profiles of slopes and valleys

Validity of the mathematical expressions (2.14), (2.15) and (2.17) has been confirmed in real and experimental landforms, mainly by the coincidence of the amount of landform change.

(1) Laboratory experiment on slope erosion

Experiments on gully erosion caused by simulated rainfall were conducted on a heaped up slope composed of volcanic ash. The slope was 4.3m long, 2m wide and at an angle of 24 degrees. Gullies were formed by rainfall at an intensity of 80mm per hour. The gullies extended upwards from base of the slope with decreasing speed as the time went on. Slope materials transported from the gullies deposited like a fan around the base of the slope. The average amount of erosion depth or deposition depth was measured at each cross section, set at 10 or 20cm intervals. Longitudinal changes in the average amount of erosion depth or deposition depth, in other words, the changes in the longitudinal profiles of average slopes, coincide well with those calculated by the equation (2.14). The values m and C ($=k_1/k_2$) are given by multiple

regression analysis.

Mizutani, T. (1985): Experimental study on the longitudinal profile of an artificial slope composed of volcanic ash due to gullying. Geograph. Rep. Tokyo Metropol. Univ. No. 20, 179-187.

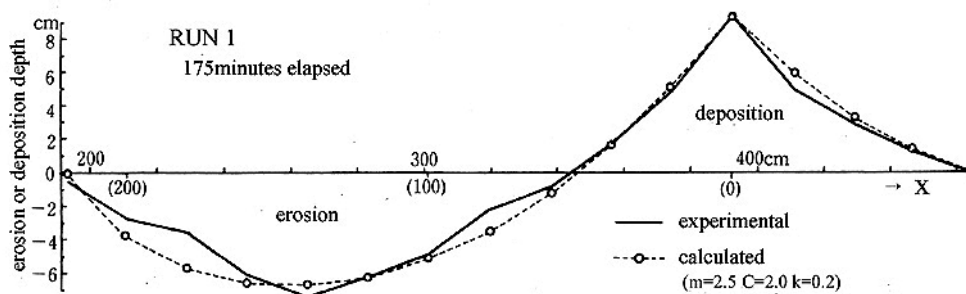


Fig. 2.7 Comparison between measured longitudinal change in the amount of average erosion or deposition depth and that calculated by equation (2.14)

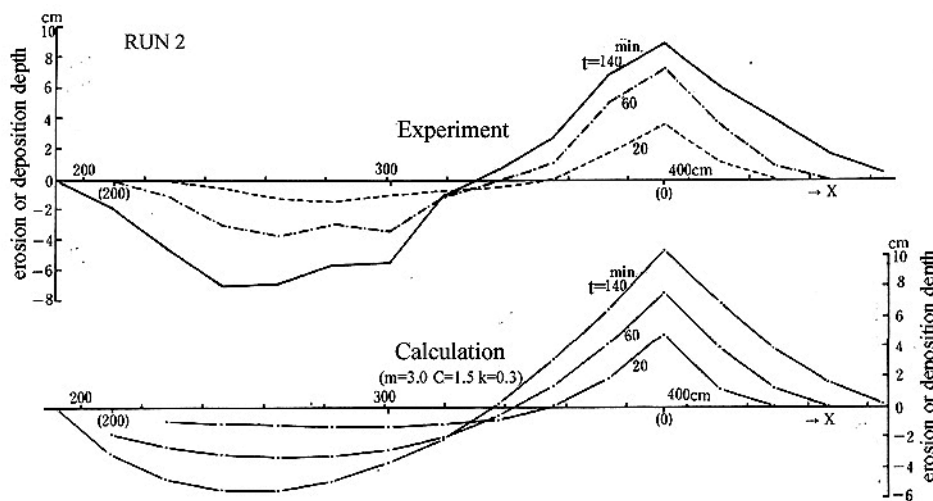


Fig. 2.8 Comparison between the measured longitudinal change in the amount of average erosion or deposition depth and those calculated by equation (2.14)

X : horizontal distance from the upper end of the slope
 Numbers in parentheses are the distance along the slope from the base of the slope

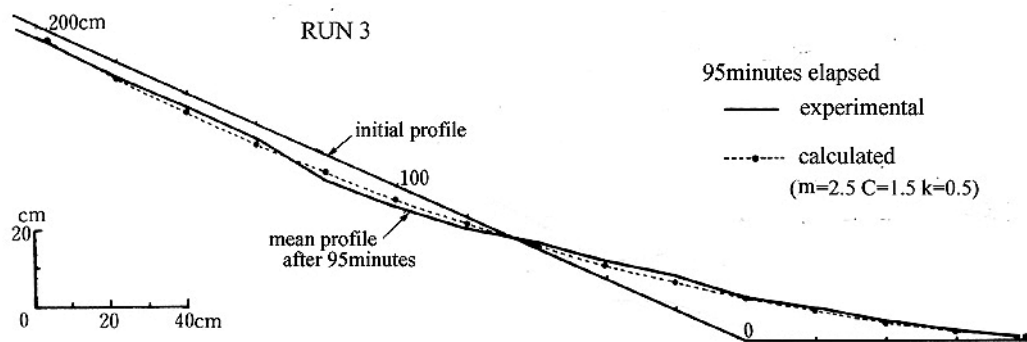


Fig. 2.9 Comparison between the measured longitudinal profile of an average slope and that calculated by equation (2.14)

(2) Valley profiles on a dissected marine terrace

On the coast of Tosa Bay, Southwestern Japan, there is a wide coastal terrace which was formed on the Last Interglacial and has been uplifted to altitudes of 150-200 m above the present sea level by crustal movement. Many valleys dissected the terrace surface with upwardly convex profiles in downstream reaches (Fig.2.10).

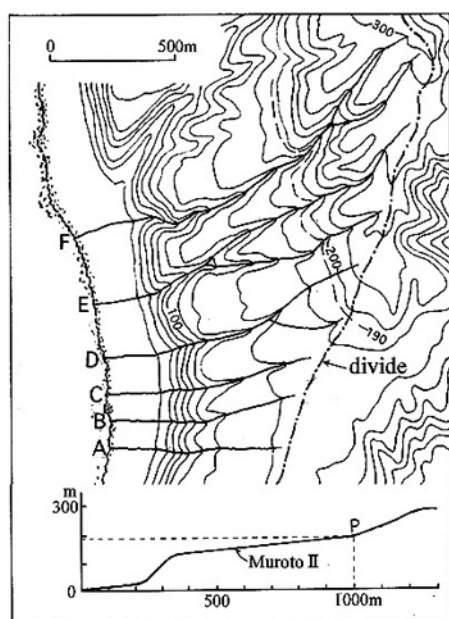


Fig. 2.10

Coastal terrace landforms in the study area on the east coast of Tosa Bay in Shikoku, Southwestern Japan. A - F are the valleys studied. below is a representative cross-section showing the terrace landform. P is where the shoreline was located 125,000 years ago.

Numerical simulations were conducted to investigate the development of longitudinal profiles of the valleys under the influence of base level change and marine erosion. A time sequence of seashore migration which has been caused by marine erosion and relative sea level change due to crustal uplift and glacial eustasy since the Last Interglacial was given as a boundary condition. Numerical calculations were conducted using a finite difference method, starting from 125,000 years ago when the shoreline was located at the upper end of the terrace surface, and progressive changes in the valley profiles over time were simulated. The present

profiles obtained from the calculation fit quite closely to actual valley profiles, which demonstrates the validity of the basic equation, and at the same time suggests a formation process for wide coastal terraces.

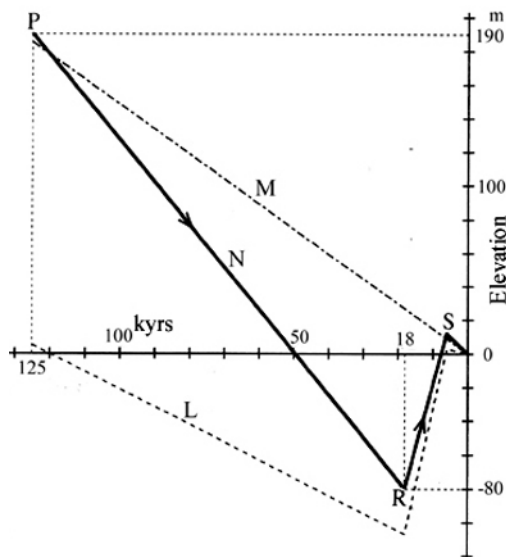


Fig. 2.11 Temporal changes in relative sea level in the study area since the Last Interglacial caused by glacial eustasy and crustal uplift

Horizontal axis is thousands of years before the present. Line L shows simplified sea level change due to glacial eustasy. Line M shows sea level fall relative to the land caused by continuous uplift. Solid line N is the sum of the other two. The rate of relative sea level change during $P \rightarrow R$ and $R \rightarrow S$ were -2.5mm/yr and 7.6mm/yr respectively.

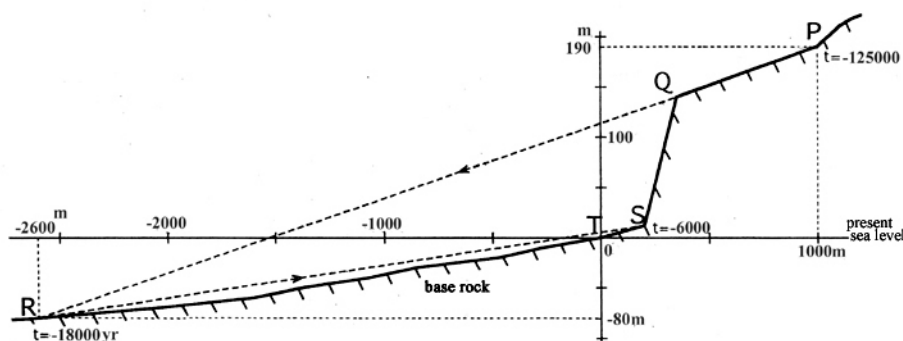


Fig. 2.12 Temporal changes in the location of the shoreline in the study area since the Last Interglacial.

Horizontal axis is the distance from present seashore T. S.L. is present sea level. It is supposed that shoreline was located at P 125,000 years ago, at R 18,000 years ago, and at S 6000 years ago. The bed rock under the sea is partly covered with sandy layer less than 20 m thick. From the profile of the bedrock surface under the sea obtained from geologic map, it is derived that the shoreline at the lowest sea level 18,000 years ago progressed far offshore, more than 2600 m. S is the inner edge of bedrock surface at the foot of the cliff, with the altitude of 12 meters.

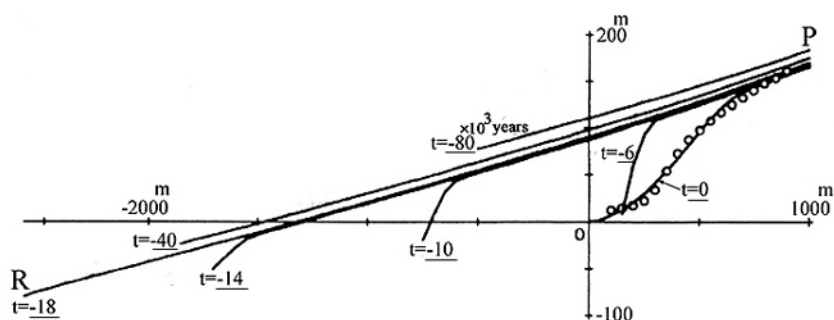


Fig.2.13 Development of the longitudinal profile of valley F since the Last Interglacial. The head of valley F is located 550m upstream of P. Solid lines are calculated profiles at the time shown by the underlined numbers. In the regression phase after the Last Interglacial, the valley channel extended seawards in an almost straight line from P to R, shallowly down-cutting the newly exposed land. At $t = -18000$ the valley mouth reached R. In the transgression stage after the Last Glacial Maximum, the valley profile in downstream reaches became highly convex by the rapid retreat of the valley mouth. After $t = -6000$ when the profile was most convex, smoothing of the profile occurred. Open circles show the measured profile.

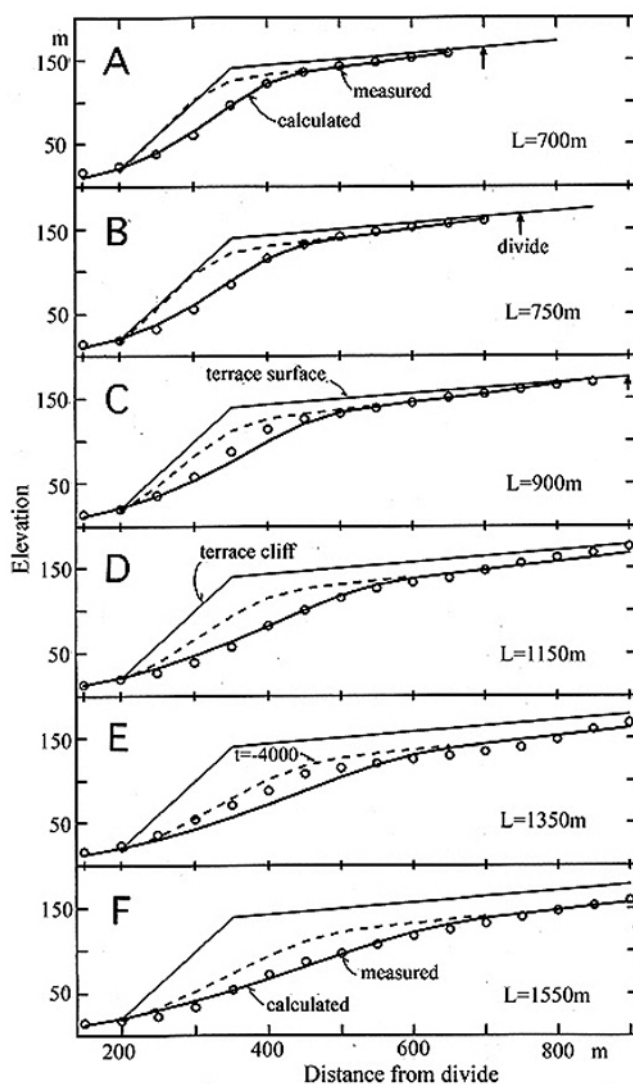


Fig.2.14 Comparison of the measured valley profiles (open circles) with the calculated (solid lines) for six valleys A-F having various values of L .

The value L is the distance from the divide to the shoreline. Arrow shows the location of the divide. Dashed lines are the calculated profiles at $t = -4000$ yr. For comparison the profiles of the original terrace surface and that of the present sea cliff are shown by fine solid lines.

Mizutani, T. (1996): Longitudinal profile evolution of valleys on coastal terraces under the compound influence of eustasy, tectonism and marine erosion. *Geomorphology* 17, 317-322.

(3) Erosional development of mountain slopes

Basic equations used for calculation are

$$q = a(xS)^3 \quad (2.23)$$

$$\frac{\partial z}{\partial t} = -k \frac{\partial q}{\partial x} \quad (2.24)$$

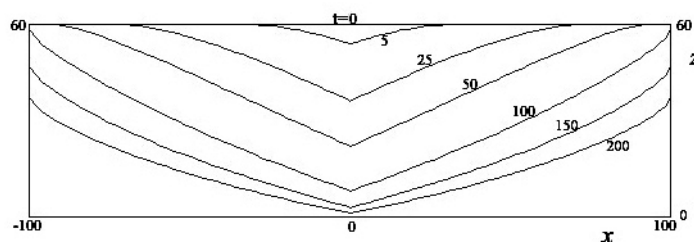


Fig.2.17 Evolution of valley cross section

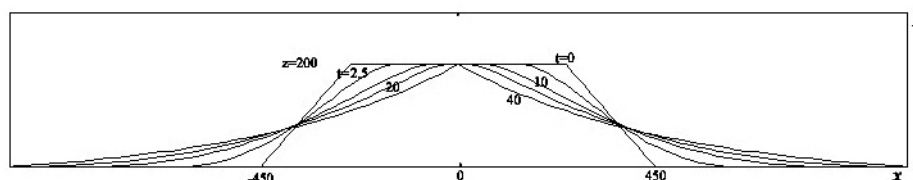


Fig.2.18 Evolution of mountain slope

2.3 Alluvial fans

From a simplified hydraulic mechanism of sediment transport on open fan surfaces, it is derived that the gradient of a fan surface can be expressed by a power function of the distance from the fanhead. The exponent represents the convexity or concavity of the longitudinal fan profile. The existence of the relation expressed by the power function has been recognized in many small natural fans and laboratory fans. In some natural fans the exponents change at certain points in midfans. The changes are inferred to have been caused by the spread of water flow on the fan surface and by locational differences of the transporting agents. This inference is supported by laboratory experiments and theoretical modelling.

Mizutani, T. (1986): Longitudinal change in the gradient of alluvial fan surfaces. Geograph. Rep. Tokyo Metropol. Univ., No.21, 251-260.

(1) Longitudinal fan surface profile

Basic equations are as follows.

Continuity equation of sediment load:

$$\frac{\partial z}{\partial t} = -\frac{1}{w(1-\lambda)} \frac{\partial(q_b w)}{\partial x} \quad (2.25)$$

Tractional load:

$$q_b = c\tau^\alpha = c(\rho ghS)^\alpha \quad (2.26)$$

Equation of motion of water flow:

$$q = \frac{1}{n} h^{5/3} S^{1/2} \quad (2.27)$$

Equation of continuity of water flow:

$$\frac{d(qw)}{dx} = 0 \quad (2.28)$$

$$w = px + w_0 \quad (2.29)$$

From these equations the following relation is derived.

$$\frac{\partial z}{\partial t} = K \frac{S^{\alpha-1}}{(px + w_0)^{1+0.6\alpha}} \left\{ (1 - 0.6\alpha)pS + (px + w_0)\alpha \frac{\partial S}{\partial x} \right\} \quad (2.31)$$

$$K = -\frac{c\rho^\alpha g^\alpha}{1-\lambda} \left(\frac{nQ_0}{S^{0.5}} \right)^{0.6\alpha}$$

In a steady state, that is, when $\partial z / \partial t = 0$

$$(1 - 0.6\alpha)pS + (px + w_0)\alpha \frac{dS}{dx} \quad (2.32)$$

is derived. Solving the equation, the following equation which describe longitudinal fan surface profile is obtained.

$$S = S_0 px^{(0.6\alpha-1)/\alpha} \quad (2.33)$$

This shows that relationship between x and S is linear on a log-log paper.

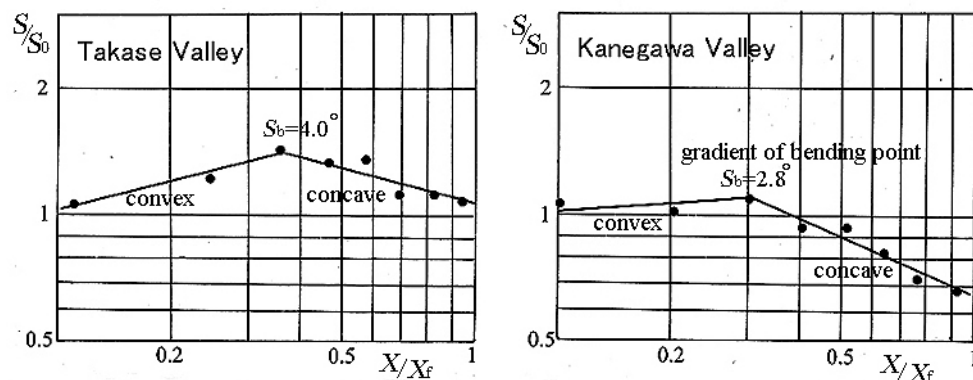


Fig.2.20 Relationship between surface gradient (S/S_0) of natural fan and distance (X/X_f) from fanhead
 S_0 : gradient of fanhead X_f : distance from fanhead to toe

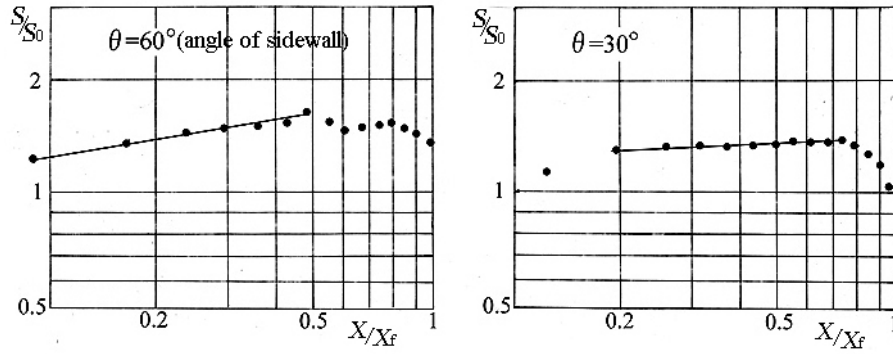


Fig.2.21 Relationship between surface gradient (S/S_0) of laboratory fan and distance (X/X_f) from fanhead

(2) Digital simulations

Basic equations are

$$\frac{\partial(uh)}{\partial t} = -gh \frac{\partial(h+z)}{\partial x} - gn^2 \frac{u|u|}{h^{1/3}} \tag{2.34}$$

$$\frac{\partial(vh)}{\partial t} = -gh \frac{\partial(h+z)}{\partial y} - gn^2 \frac{v|v|}{h^{1/3}} \tag{2.35}$$

$$\frac{\partial z}{\partial t} + \frac{\partial q_{bx}}{\partial x} + \frac{\partial q_{by}}{\partial y} = 0 \tag{2.36}$$

$$q_{bx} = q_{by} = K(\rho gh \sin \theta)^3 \tag{2.37}$$

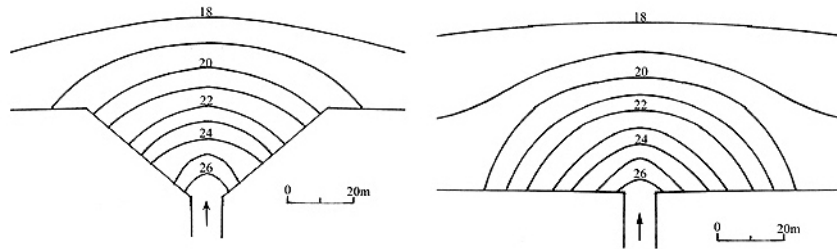


Fig.2.22 Simulated fans by Eqs.(2.34), (2.35) and (2.36)

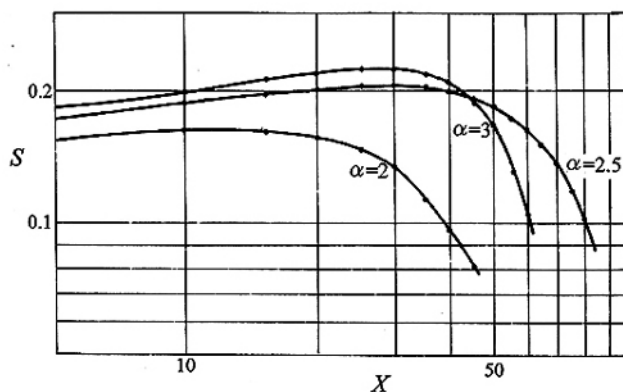


Fig.2.23 Relationship between gradient (S) of fans simulated by Eq.(2.31) and distance (X) from fanhead α : exponent of (2.31)

2.4 River terraces

(1) Flume experiments

The formation mechanism of multiple erosional terraces which develop in the dissection process of sedimentary valley fills was investigated by laboratory experiments and computer simulations. Sequences of unpaired terraces were produced on experimental fan-like deposits under condition of constant water discharge, no base-level change, and no sediment supply (Fig.2.25). The terraces developed as a result of the repetition of lateral shifting and still-stand of the stream channel at each cross-section during continuous down-cutting (Fig.2.27). This mode of channel migration was caused by meander growth during which amplitude and wavelength increased with time.

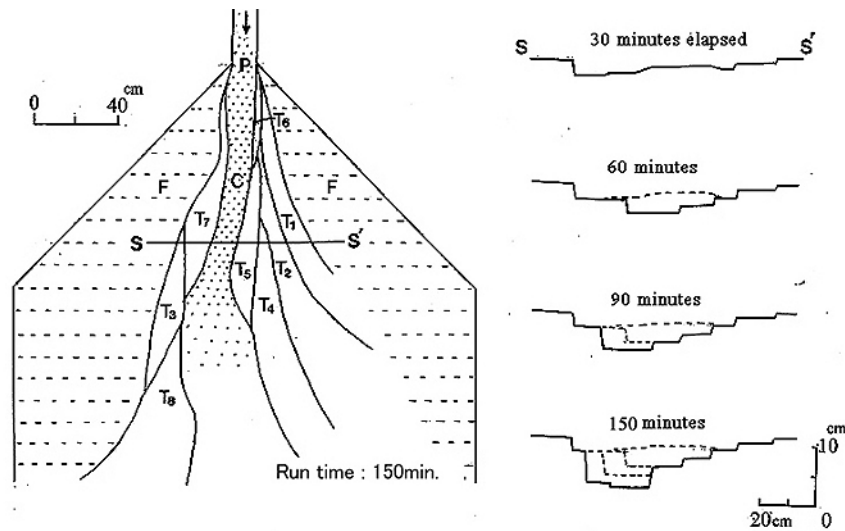


Fig.2.25 Spatial distribution and transverse profiles of terraces formed in a laboratory experiment in which multiple terraces are well developed
 F : original fan surface, T₁--T₈ : erosional terraces, C : final stream channel.
 Transverse profiles are those in cross-section S--S'.

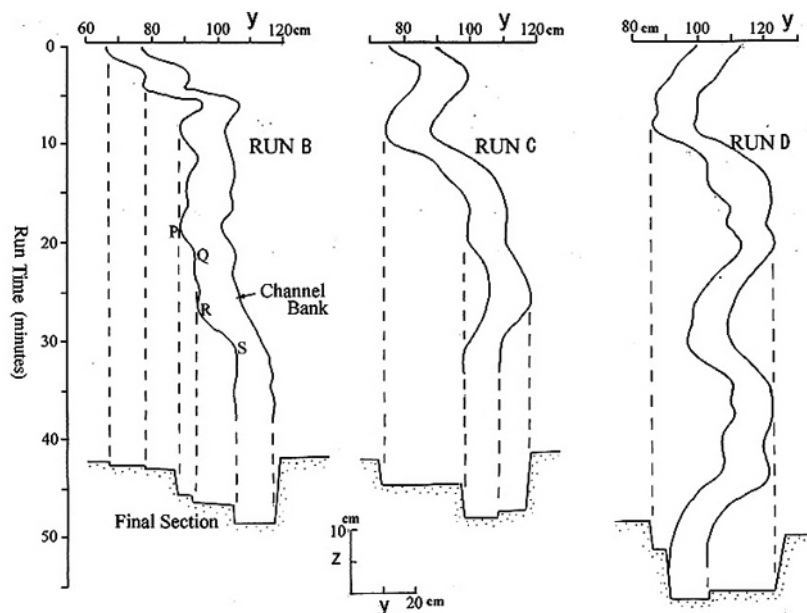


Fig.2.27 Changes in transverse location of channel banks with time and final terrace profiles in cross-section S--S' observed in laboratory experiments.
 P--Q, R--S : lateral shifting phase, Q--R : still stand phase.

(2) Computer simulations

Terrace formation processes observed in the laboratory experiments were reproduced by computer simulations using a simple meander model. The meander channel is represented by a sine curve in which amplitude and wavelength are functions of time and distance from the fan apex:

$$y = A \sin(2\pi x / C) \quad (2.38)$$

$$A = (12 + 4t - 0.01x)K, \quad C = 120 + 100t + 0.5x$$

where x is the distance from the fan apex along the midline of the deposition area, y is the transverse distance from the midline, A is the amplitude, C is the wavelength, t is time, and K is a coefficient.

The terraces developed by intermittent lateral channel shifting caused by meandering growth in which amplitude and wavelength increased with time. The meandering growth mode may prevail on fairly steep valleys infilled with alluvial deposits, as well as on alluvial fans. External stimuli such as climatic variation, tectonism or base-level change are the factors which primarily affect the rate of vertical incision. Since terrace surface is a former river channel, an explanation of the origin and mode of lateral channel shifting is essential for clarifying the mechanism of multiple terrace formation.

Mizutani, T. (1998): Laboratory experiment and digital simulation of multiple fill-cut terrace formation. *Geomorphology*, 24, 353-361.

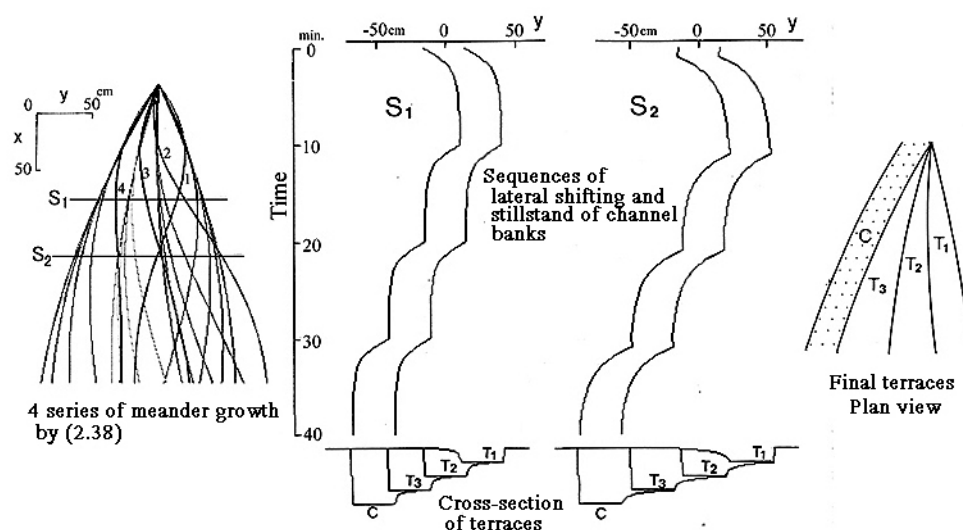


Fig.2.30 Simulated channel pattern growth and the resulting terraces (1)

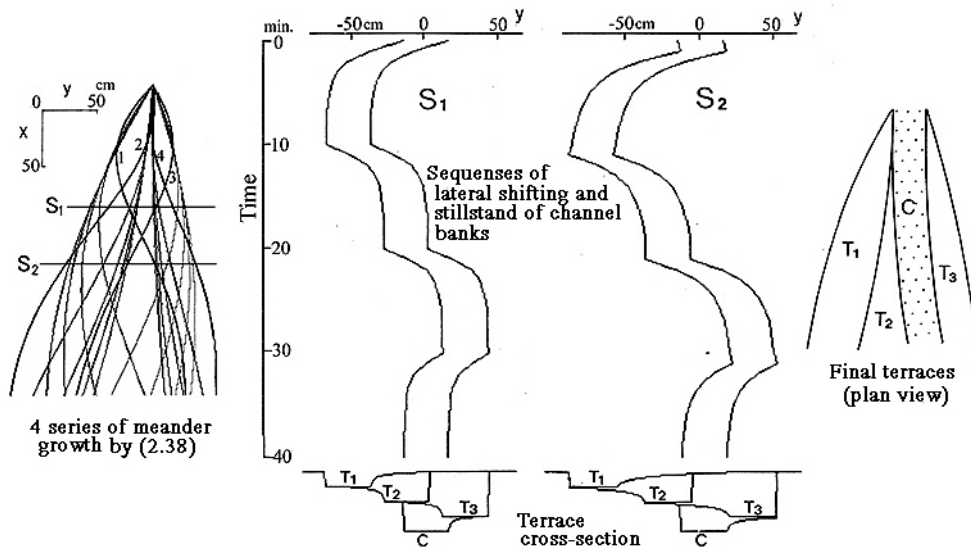


Fig.2.31 Simulated channel pattern growth and the resulting terraces (2)

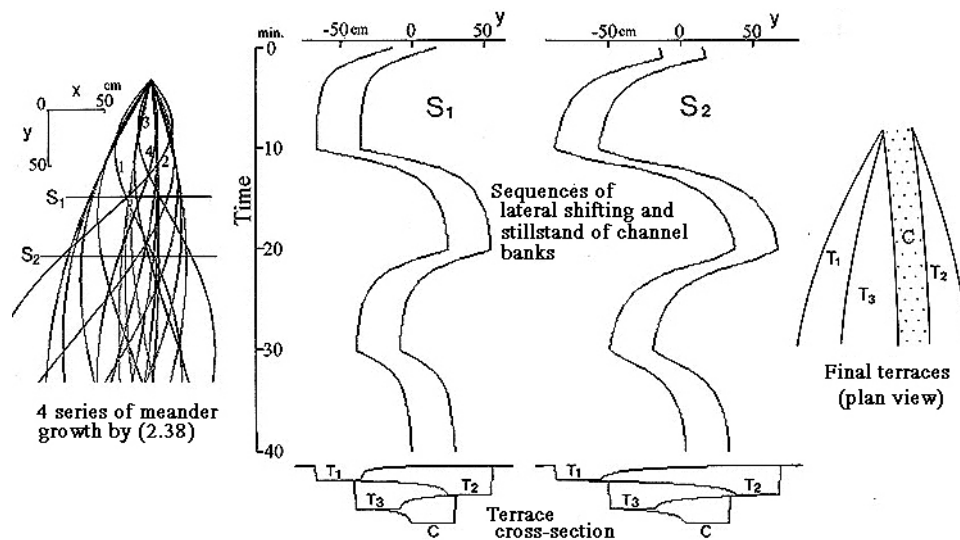


Fig.2.32 Simulated channel pattern growth and resulting terraces (3)

2.5 Drainage basin and stream network

(1) Erosion rate

Regression equations for estimating the amount of sediment discharge from steep mountain basins have been derived by using 43 data of sedimentation in sabo-dams in Central Japan. One of the regression equations is

$$q_s = 1.862 \times 10^{-2} S^{3.74} P_3^{2.97} K \quad r=0.944 \quad (2.39)$$

where q_s : the amount of sedimentation in a sabo-dam per a unit drainage basin and per year, S : mean basin gradient, P_3 : maximum 3-hour rainfall intensity, K : geologic coefficients which are obtained by using dummy variables.

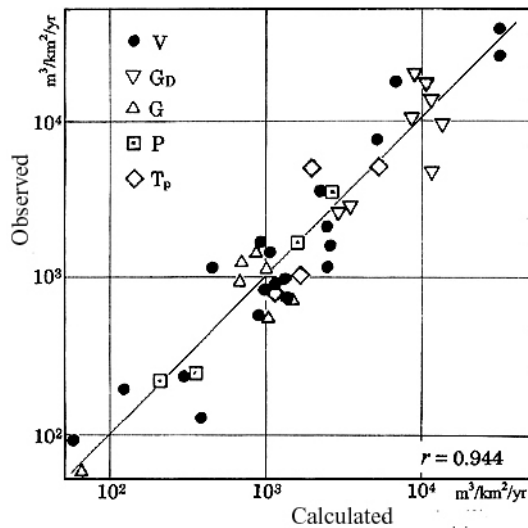


Fig.2.33 Relationship between surveyed q_s and the calculated by Eq.(2.39)

Geologic coefficients when that for volcanic rocks (V) is set at 1 are 0.22 for granitic rocks (G), 0.35 for palaeogene sedimentary rocks (T), 0.14 for Palaeozoic rocks (P) and 1.04 for granitic rocks suffered from pollution by mining (G_D). K represents the relative resistivity to erosion.

(2) Drainage basin development

Erosional development of mountain basins has been simulated by using digital elevation data in a 50m mesh. Gradients to neighbouring 8 meshes are measured by each mesh. The amount of sediment transport to the mesh with maximum gradient is calculated by

$$q = K_1(AS) + K_2(S - S_0) \quad (2.41)$$

where q is the amount of sediment transport, A is catchment area upstream of each mesh (number of inflow mesh), S is gradient, S_0 critical gradient, and K_1, K_2 are

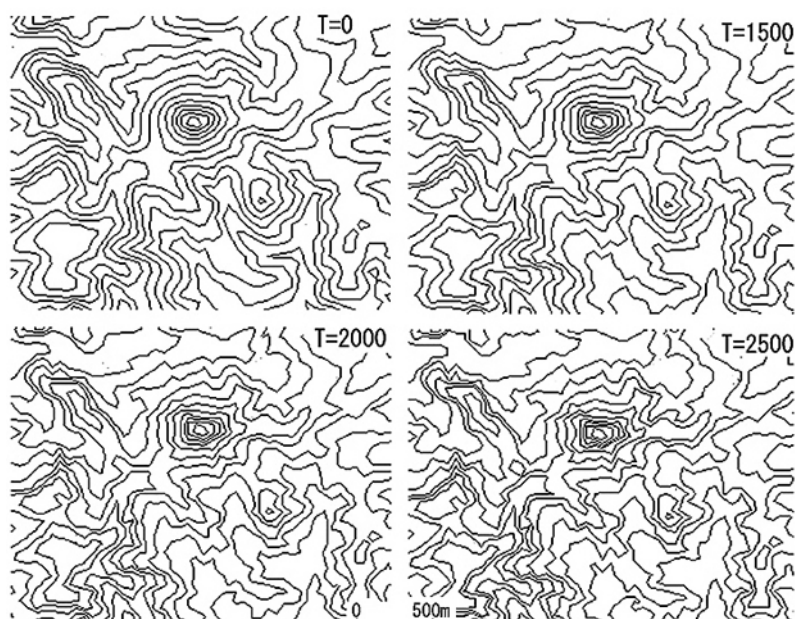


Fig.2.34 Sequence of simulated contour maps (Soya Hills, Hokkaido) Contour interval is 10 meters. Upper left (T=0) is the present map. The maps are drawn by using digital elevation data at each time step.

proportional constants. The first term represents the transport by running water and the second term by mass wasting.

At first sediment transport to maximum gradient direction is calculated for every mesh. Then, erosion depth or deposition depth is calculated by the following continuity condition for every mesh.

$$\Delta z = \frac{1}{\Delta x \Delta y} (q_{in} - q_{out}) \quad (2.42)$$

where Δz is erosion or deposition depth, Δx , Δy are mesh interval, q_{in} sediment inflow, q_{out} sediment outflow. By these calculations digital elevation data after Δt time step is obtained. Again, by using the new digital elevation data, the same calculation is executed. Fig.2.34 is an example of simulated landscape evolution. T is the number of calculation step.

The validity of the simulation has been confirmed by the law of stream networks. The test field is the Soya hills in Northern Hokkaido which is composed of Tertiary sedimentary rocks slightly dissected by shallow valleys. Stream networks are drawn on contour maps prepared from simulated digital elevation data (Fig.2.36).

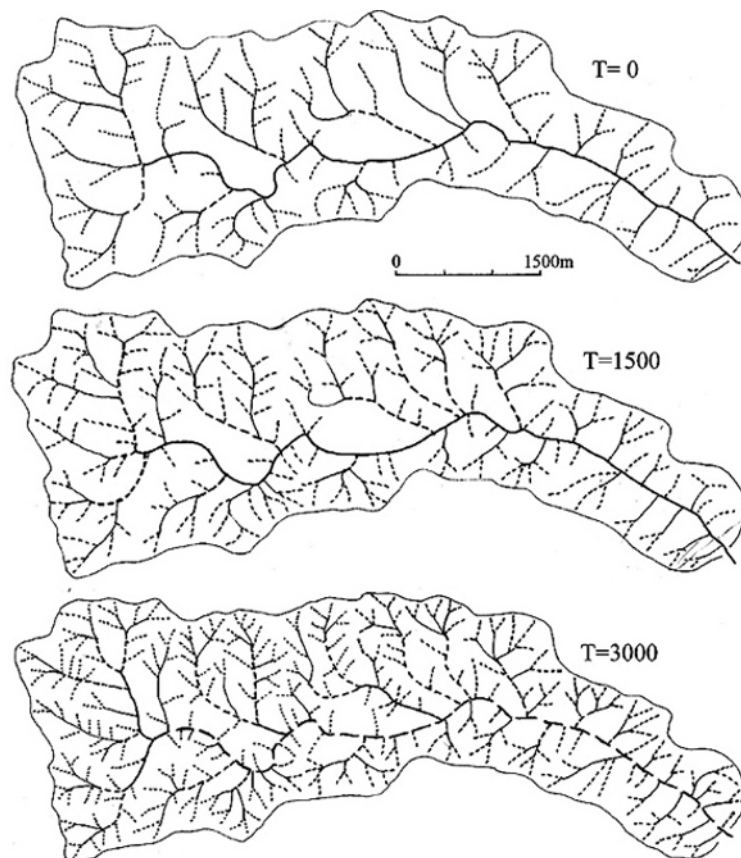


Fig.2.36 Simulated sequence of drainage networks
(Onishibetsu River, Northern Hokkaido)

The networks are drawn on contour maps prepared from simulated digital elevation data at each time step.

The relationship between stream order and the number of stream is almost linear throughout the time, that is, law of stream number is realized at every step (Fig.2.38).

Bifurcation ratio keeps almost a constant, about 3.8. At T=3000 maximum stream order increased by 1. As the lapse of time, drainage density increases linearly, as a result of the increase in the number of short low order stream. T=1000 is supposed to be about 10 thousands years.

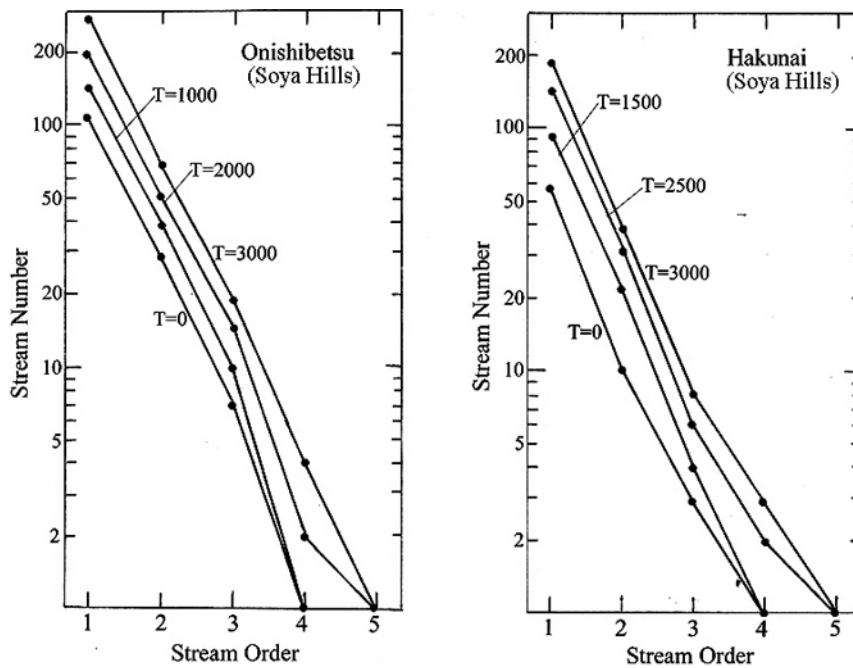


Fig.2.38 Changes of the relationship between stream order and stream length with time obtained from simulated stream networks.

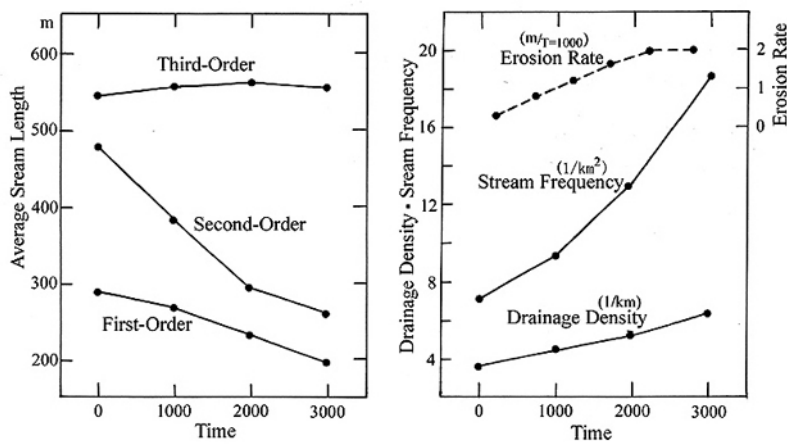


Fig.2.39 Change of simulated basin properties with time



Fig.2.41

Simulated distribution of erosion depth after T=2500 at Mt.Rishiri, Northern Hokkaido. Mt.Rishiri is strato-volcano with the altitude of 1719 m.
 black:more than 30 m
 gray:10 - 30 m
 blank:less than 10 m